Journal of Ultrafine Grained and Nanostructured Materials
https://jufgnsm.ut.ac.ir
Vol. 55, No.1, June 2022, pp. 21-30
Print ISSN: 2423-6845 Online ISSN: 2423-6837
DOI: 10.22059/jufgnsm.2022.01.04

Photocatalytic properties of ZnO/CuO nanocomposite prepared in acidic media

Nargol Jalali[1], Mohammad Nami[1], Fereshteh Rashchi*[,1], Amirhossein Rakhsha[1,2]

[1]School of Metallurgy and Materials Engineering, College of Engineering, University of Tehran, Tehran, Iran;
[2]Department of Chemical Engineering, McMaster University, Hamilton, Ontario, Canada.

Recieved: 11 October 2021; Accepted: 11 March 2022

**Corresponding author email: rashchi@ut.ac.ir*

ABSTRACT

In this work, the ZnO/CuO nanocomposite was synthesized with two different initial pH values in an acidic media through a simple one-step and cost-efficient chemical bath precipitation method. To alter the pH value of the solution, nitric acid was added dropwise and initial pH values were 1.5 and 4.5, respectively. The crystal phase structure of the samples was investigated by X-ray diffraction analysis (XRD), indicating the formation of wurtzite structure of ZnO and monoclinic structure of CuO. Additionally, the morphological structure of the as-formed nanocomposites was studied by field emission scanning electron microscopy (FESEM). It was demonstrated that at pH = 4.5 and 1.5, ZnO nanorods/CuO nanoflakes and ZnO nanoparticles/CuO nanosheets were formed, respectively. For optical characterizations, diffuse reflectance spectroscopy (DRS) and photoluminescence (PL) spectra were performed. The band gap energy of the as-prepared samples was calculated at 3.08 and 2.9 eV with an initial pH of 1.5 and 4.5, respectively. Furthermore, PL data revealed that the sample synthesized in pH = 4.5 exhibits a significant decrease in electron/hole recombination rate compared with that of the sample fabricated in pH = 1.5. Accordingly, the photocatalytic activity of the as-prepared samples was studied employing methylene blue (MB) under visible-light irradiation. Overall, the prepared sample at pH = 4.5 and pH = 1.5 demonstrated ~76% and ~66% photo-degradation efficiency of MB after 150 min, respectively. Finally, the role of holes and hydroxyl radicals on the degradation of MB were proposed using charge carrier scavengers.

Keywords: *Photocatalysis; ZnO; CuO; Nanocomposite; Chemical bath precipitation.*

1. Introduction

Zinc oxide (ZnO) has attracted interest due to its various morphological structures as an n-type semiconductor. In addition, ZnO has a wide direct band gap of 3.37 eV [1] which makes it functional for multiple optoelectronic applications such as photocatalysis [2], solar cells [3], light-emitting diodes [4], and UV sensors [5]. Owing to the growth of population and rising water pollutants, photocatalytic applications as a practical method for water treatment have attracted interest for the past decades as a sustainable technology. In a photocatalytic system, the semiconductor particles act as oxidizing agents by producing hydroxyl radicals under light irradiation. Respectively, ZnO is highly suggested for photocatalytic applications as a low-cost and non-toxic semiconductor. However, ZnO has a high electron-hole recombination rate and due to its wide band gap energy, the electrons can only be generated under UV light irradiation which limits harvesting visible light.

Coupling ZnO with a p-type semiconductor such as CuO (with a narrow band gap energy of 1.2-1.5 eV) has been reported to be efficient to

avoid the mentioned drawbacks and enhance the photocatalytic activity by prolonging the lifetime of the photo-generated charge carriers and lowering their recombination rate. Accordingly, ZnO/CuO nanocomposites can be obtained by diverse synthesis methods including sol-gel [6], hydrothermal [7], and chemical bath precipitation (CBP) [8]. Amongst all, CBP is a facile, low-temperature method and has been widely used in the synthesis of nanostructures. Multiple studies have been done on the photocatalytic performance of ZnO/CuO nanocomposite. Xu et al.[9] synthesized CuO/ZnO nanocomposite using hydrothermal method. It was found that CuO/ZnO nanocatalysts exhibit higher photocatalytic performance in contrast to pure ZnO and CuO. Naseri et al.[10] studied the effect of CuO content on optical properties of ZnO/CuO nanocomposite and reported that at higher CuO concentrations, lower photocatalytic performance occurs due to the band gap narrowing. Accordingly, Nami et al.[11] fabricated ZnO/CuO nanocomposite through CBP method with various concentrations of CuO and reported that the ZnO/(10 mol%) CuO nanocomposite represented the highest photo-degradation of MB.

Moreover, the pH efficiency of ZnO nanorods was studied by Mwankemwa et al.[12] and Verrier et al.[13] using low-temperature CBP which indicated that the addition of ammonia decreases the density and diameter of nanorods. It is worth mentioning that the photocatalytic activity of materials highly depends on particles size which can be changed with morphology variation. Morphologies can be altered by different parameters such as temperature, time, and pH during the synthesis process. To the best of our knowledge, the influence of synthesis pH on the photocatalytic performance of ZnO/CuO nanocomposite was rarely reported. Hence, in this study, different amounts of nitric acid were used to fabricate ZnO/(10 mol%) CuO nanocomposite through a low-temperature CBP method and the effect of acidic synthesis media on photocatalytic activity of this nanocomposite was investigated.

2. Experimental Details

Zinc nitrate hexahydrate (ZNH) ($Zn(NO_3)_2.6H_2O$) as Zn precursor, copper nitrate tetrahydrate ($Cu(NO_3)_2.3H_2O$) as Cu precursor, Hexamethylenetetramine ($C_6H_{12}N_4$, HMTA) as a pH buffer and nitric acid (HNO_3) as a pH adjustment were used. All chemicals mentioned above were purchased from Merck KGaA. Furthermore, deionized water (18.2 MΩ) was utilized as the solvent in the synthesis of ZnO/CuO nanocomposite. The ZnO/CuO nanocomposite was synthesized through a chemical bath deposition method. In detail, 20 mM of ZNH, 2 mM of CN, and 20 mM of HMTA were dispersed into 320 mL of deionized water. Different amounts of nitric acid were introduced into the solution until the pH was 4.5 (CZ4.5) and 1.5 (CZ1.5). The obtained solution was placed in a water bath with a temperature of 90 ˚C under constant stirring for 3h. The precipitated powder was dried at 60 ˚C.

The crystallinity was analyzed using a Philips X-ray diffractometer (XRD) with Cu-Kα irradiation. The morphologies of the as-prepared samples were examined by field emission scanning electron microscopy (FESEM, JEOL Centurio, operated at 15 kV). The photoluminescence (PL) and the diffuse reflectance spectroscopy (DRS) spectra were measured by Varian Cary Eclipse Fluorescence Spectrophotometer and Shimadzu MPC-2200, respectively, to confirm the photoconductivity and investigate the absorption spectra of the samples.

The photocatalytic activity of the samples was investigated by degradation of 30 mL of MB solution with an initial concentration of 2 mg/L under the irradiation of visible light. The visible light was produced by a 150 W lamp (OSRAM, Germany) located at 30 cm above the solution. In order to achieve the adsorption–desorption equilibrium, the mixture of the photocatalytic powder and MB solution was stirred in dark for 30 min with a magnetic stirrer at ambient temperature. To evaluate the effect of the concentration of MB, 2 mL of the solution was extracted at an interval of 30 min at a duration span of 150 min and the samples were analyzed by UV-Vis spectrophotometer (Unico 2100 model). To estimate the dye concentration, the maximum absorption peak of MB at 664 nm was used. Moreover, the blank test was done under similar conditions. To identify the generated reactive species during the photocatalytic degradation process, radical scavenging experiments were performed. The radical scavenging activities were carried out using 10 mM of methanol (MeOH), 10 mM of disodium ethylenediamine-tetraacetate (EDTA), and 2 mM of p-benzoquinone (BQ), and 10 mM of cupric nitrate (CN). Three cycles were investigated to evaluate the stability and recyclability of the

photocatalyst through the photocatalytic process. After each cycle, the powder was washed with ethanol (98 %) and distilled water to be used again in the next cycle.

3. Results and discussion

Fig. 1 demonstrates the XRD patterns of the samples. Based on JCPDS No. 36-1451 three main peaks of wurtzite ZnO are located at the angles of 31.8, 34.4, and 36.3, which are attributed to the (100), (002), and (101) planes, respectively. Moreover, the two main peaks of monoclinic CuO are located at 35.5 and 38.8 degrees according to JCPDS No. 48-1548. The high-intensity peaks of wurtzite ZnO and monoclinic CuO were observed in the XRD pattern of the CZ4.5 sample. To clarify the formation mechanism of ZnO and CuO, it should be noted that the OH^- produced from the hydrolysis of HMTA according to the equations 1 and 2, reduces the concentration of H^+ ions and reacts with Zn^{2+} and Cu^{2+} to form intermediate hydroxides through equations 3 and 4 [14].

$$(CH_2)_6N_4 + 6H_2O \leftrightarrow 6HCHO + 4NH_3 \quad (1)$$

$$NH_3 + H_2O \leftrightarrow NH_4^+ + OH^- \quad (2)$$

$$Zn^{2+} + OH^- \rightarrow Zn(OH)_2 \quad (3)$$

$$Cu^{2+} + OH^- \rightarrow Cu(OH)_2 \quad (4)$$

These intermediate complexes act as growing units to form ZnO and CuO as follows [15]:

$$Cu/Zn(OH)_2 \leftrightarrow Cu/ZnO + H_2O \quad (5)$$

On the other hand, in a highly acidic solution, the XRD peak intensities of ZnO and CuO decreased. To be more specific, increasing the concentration of nitric acid increases the amount of H^+ ions produced. Therefore, the excessive H^+ ions combine with negatively charged OH^- ions and restrict the formation rate of ZnO and CuO crystals in the CZ1.5 sample [16].

The FESEM images of as-prepared samples are presented in Fig. 2. Sample CZ1.5 reveals ZnO nanoparticle and CuO nanosheets as shown in Fig. 2a. HMTA plays an important role as a surfactant in the formation of CuO nanosheets according to the hydroxyl ions generated from the decomposition of HMTA [17]. Moreover, the high concentration of H^+ ions tends to slow the formation rate of $Zn(OH)_2$ via equation 3 by restricting the number of OH^- ions. Thus, the limited precipitation rate of ZnO leads to the formation of ZnO nanoparticles [18]. With a small amount of nitric acid and increasing the pH to 4.5, ZnO nanorods and CuO nanoflakes are formed according to the FESEM images of the CZ4.5 sample in Fig. 2b. The shape-inducing effect of HMTA causes the formation of ZnO nanorods in which attaching to the non-polar planes of wurtzite ZnO leads to the growth along the polar (basal) plain of ZnO [19]. Liao et al. [20] reported when the hydrogen bonds formed between $Cu(OH)_2$ molecules were not aligned directly, $Cu(OH)_2$ molecules can be deposited in distinct ways and form nanoflakes. Through dehydration of $Cu(OH)_2$ (Eq. 5), CuO nanoflakes tend to form. The corresponding elemental mapping images confirmed the presence of Cu and Zn in each sample. In addition, the selected areas in the Cu and Zn mapping of the samples indicate the positions of CuO and ZnO nanostructures, respectively. Accordingly, these areas are brighter in the Cu element maps and conversely darker in Zn mapping. The homogeneous dispersion of the

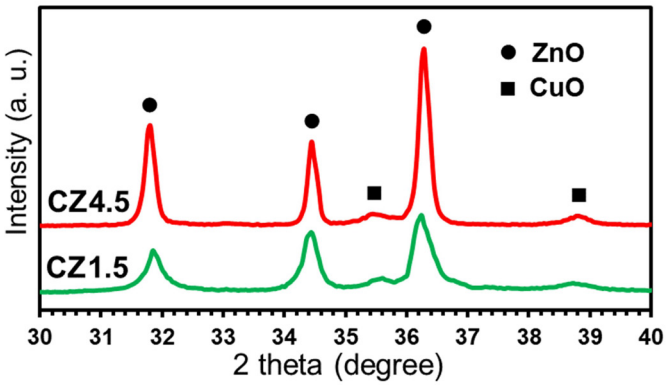

Fig. 1- XRD patterns of the samples.

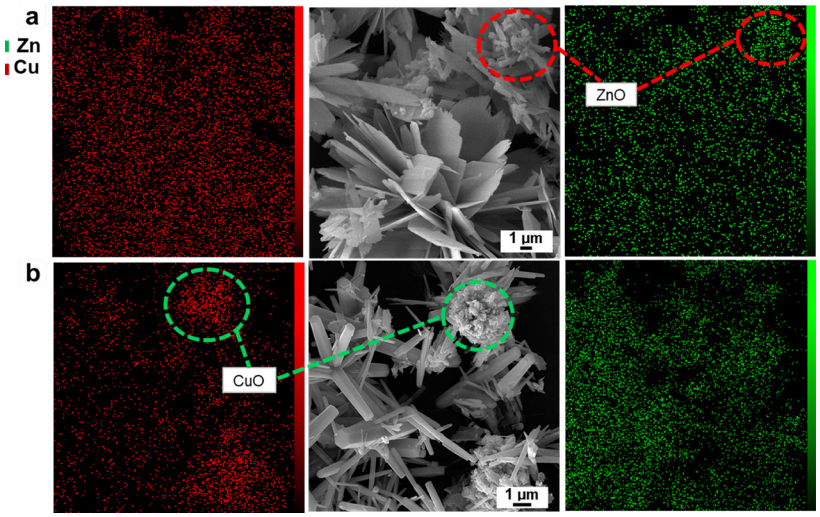

Fig. 2- FESEM images of (a) CZ1.5 and (b) CZ4.5 and the corresponding Cu and Zn mapping images.

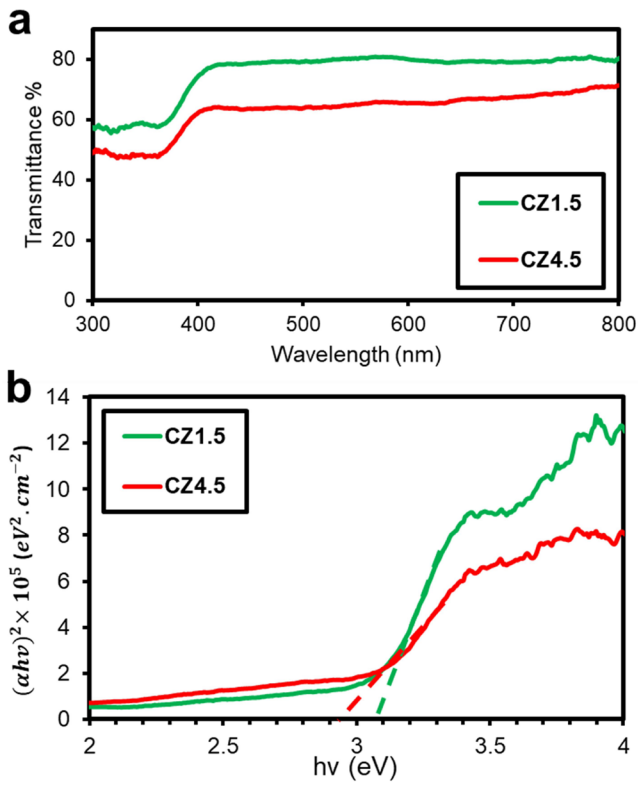

Fig. 3- (a) DRS plot and (b) Tauc plots of the samples.

elements in both samples could be attributed to the unintentional Cu-doping [21]. Moreover, the distribution of Zn and Cu elements verified that no other impurities are presented in the as-synthesized nanocomposites.

The DRS analysis of the synthesized samples evaluated in the range of 300-800 nm is presented in Fig. 3a. A broad peak was appeared at around 400 nm for both samples which is attributed to the presence of Cu element [22]. The absorption edge of the CZ4.5 sample was slightly shifted to the left as compared to the CZ1.5 sample. The band gap energy (E_g) of as-prepared samples was determined using the Tauc plot (Fig. 3b) by extrapolating the linear portion of $(\alpha h\nu)^2$ to the photon energy axis. The relationship between band gap energy and

optical absorption was calculated by the following equation [23]:

$$(\alpha h\nu)^n = A(h\nu - E_g) \quad (6)$$

where α, hυ, and A are absorption coefficient, photon energy, and the proportionality constant for semiconductor materials, respectively. The value of n is found to be 2 for direct and 0.5 for indirect semiconductors [24]. The band gap energies of CZ1.5 and CZ4.5 samples were estimated at 3.08 and 2.9 eV, respectively. The morphological variation of the samples due to the change in pH value is the reason for the difference in band gap energies [25]. To be more specific, the larger E_g of ZnO nanoparticle compared to ZnO nanorods leads to the larger band gap energy of the CZ1.5 sample compared with the CZ4.5 sample [26].

Fig. 4 shows the PL spectra of the CZ1.5 and CZ4.5 samples prepared at an excitation wavelength of 325 nm. A UV peak at ~385 nm was observed which is attributed to the exciton transition between the conduction band contain Zn^{2+} (3d) and the valence band constituted by O^{2-} (2p) [27]. The PL peak position of the CZ4.5 sample is lower than the CZ1.5 sample. The reduction of peak intensity represents diminution in the recombination rate of photogenerated electron-hole pairs, resulting in higher photocatalytic activity. The improvement in peak intensity of the CZ1.5 sample was observed. Siddiqui et al. [28] investigated the optical properties of CuO nanostructures synthesized at different concentrations of citric acid and reported that the variation in PL intensities is attributed to the passivation of surface defects such as oxygen vacancies or Cu interstitials.

3.1. Photocatalytic results

Fig. 5 exhibits the photocatalytic efficiency of the CZ1.5 and ZC4.5 samples. The Photo-degradation rate of MB was evaluated by the following equation [29]:

$$W\% = \frac{C_0 - C}{C_0} \times 100 \quad (7)$$

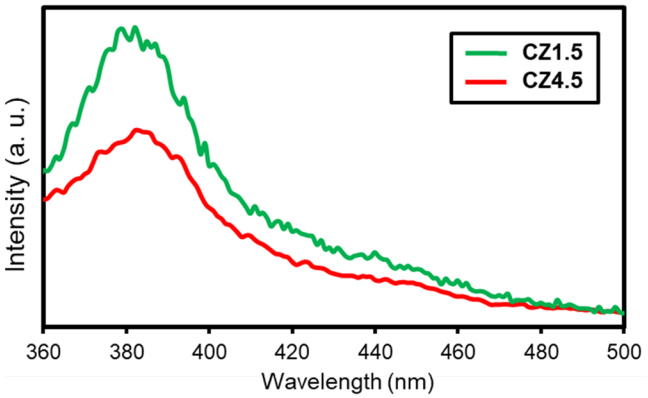

Fig. 4- PL spectra of the as-prepared samples.

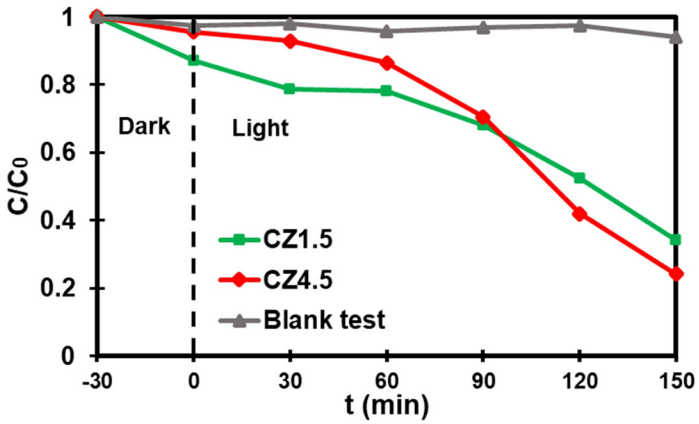

Fig. 5- Photo-degradation of MB in the absence and presence of catalyst.

where W, C, and C_0 represent the photo-degradation rate, the concentration of MB before the expositor of light, and the concentration of MB at time t. It can be seen that ~66% and ~76% of MB can be degraded after 150 mins, using the CZ1.5 and CZ4.5 samples, respectively. The blank test indicates that the degradation of MB under the irradiation of visible light is very low which can be negligible. Since the band gap energy of the CZ4.5 sample is narrower than that of the CZ1.5 sample, the CZ4.5 sample is more light-active than the CZ1.5 sample. Moreover, according to the PL analysis, the electron/hole separation is more efficient in the CZ4.5 sample in comparison with the CZ1.5 sample. Hence, the higher photocatalytic activity of the CZ4.5 sample can be attributed to these two parameters. It is worth mentioning that the saturation of active sites on the surface of the photocatalyst particles with the dye molecules can affect the photocatalytic performance of the samples [30]. This can be a reason for the dislocation in the degradation process of MB by the two samples after 90 min of irradiation.

The photocatalytic degradation mechanism is explained by the following equations [31]:

$$h^+ + H_2O \rightarrow H^+ + \cdot OH \quad (8)$$

$$e^- + O_2 \rightarrow \cdot O_2^- \quad (9)$$

$$\cdot OH/\cdot O_2^- + MB \rightarrow HO_2 + CO_2 \quad (10)$$

The degradation mechanism of MB by the ZnO/CuO nanocomposite is explained through the proposed schematic view shown in Fig. 6. Under visible light irradiation, CuO can be excited to form the electron-hole pairs. The generated electrons probably react with dissolved oxygen molecules and produce reactive oxygen species such as hydroxyl radicals (·OH) and superoxide radicals $\cdot O_2^-$ to decompose organic pollutants [32]. The oxidation of organic pollutants was conducted by the reaction of these oxidative species and the MB molecules were mineralized to harmless CO_2 and H_2O and the concentration of MB decreased.

The dosage of the catalyst is one of the most important parameters on the degradation process. The degradation efficiency was enhanced from 76% to 94% with increasing the catalyst dosage from 500 mg/L to 600 mg/L, as presented in Fig. 7. The presence of active sites on the catalyst surface is being raised and more radicals were expected to be generated. Whereas, when the catalyst dosage further increased to 700 mg/L, the trend was observed to be declined because of the scavenging effect of radicals during the reaction between excessive active sites and the (·OH) radicals [33].

In order to indicate the role of active species in the photocatalytic degradation of MB, different scavengers including CN, EDTA, MeOH, and BQ were used as the trapping agents to capture the electrons, holes, ·OH, and $\cdot O_2^-$, respectively [34]. Fig. 8(a) shows that the degradation of MB reached 68, 62, 26, and 17% in the presence of CN, BQ, MeOH, and EDTA, respectively. The degradation rates were recorded based on 150 min of reaction time. The

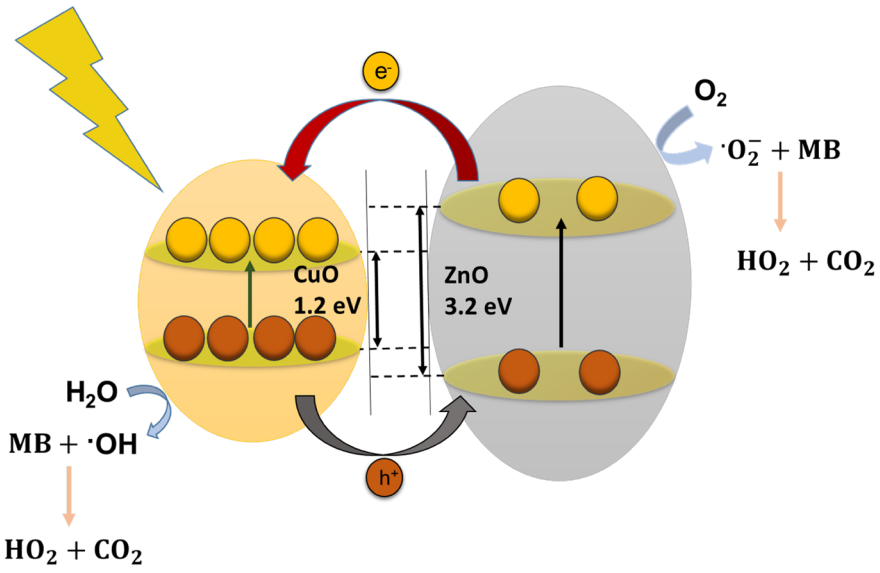

Fig. 6- Proposed mechanism of MB degradation by ZnO/CuO nanocomposite.

achieved degradation efficiency of MB shows that the addition of MeOH and EDTA had a higher impact compared to the two other scavengers. Thus, it can be concluded that the photo-generated holes are more effective than the photo-generated electrons. These results also have been confirmed by the kinetic study of the degradation process illustrated in Fig. 8(b). The kinetic study reveals that the photo-degradation of organic pollutants follows the pseudo-first-order model according to the following equation [35]:

$$\ln(C_0/C) = k_{app}\, t \quad (11)$$

where C and C_0, are the reaction concentration at time t and the initial concentration of MB, respectively, and k_{app} is the pseudo-first-order kinetic constant. Accordingly, the addition of CN and BQ resulted in a slight decrease of k_{app} to the values of 0.0076 and 0.0064 (1/min), respectively. The contribution of holes in the degradation process of MB can result in the production of •OH. Furthermore, MB dye is positively charged and because of the electrostatic force, •OH becomes adsorbed on the surface of MB and causes MB to degrade [36]. Therefore, the holes and •OH exhibit a superior effect on the photo-degradation of MB.

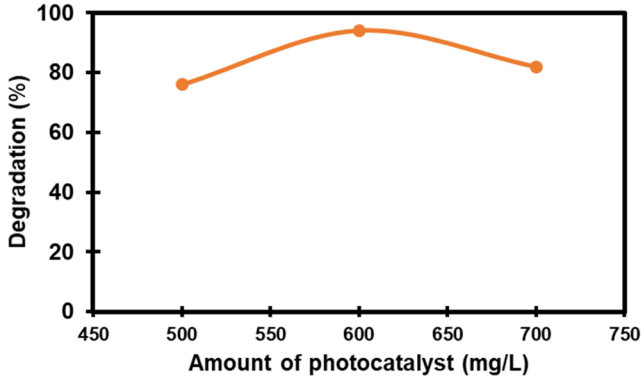

Fig. 7- Effect of catalyst dosage on photo-degradation of MB dye after 150 min of visible light irradiation.

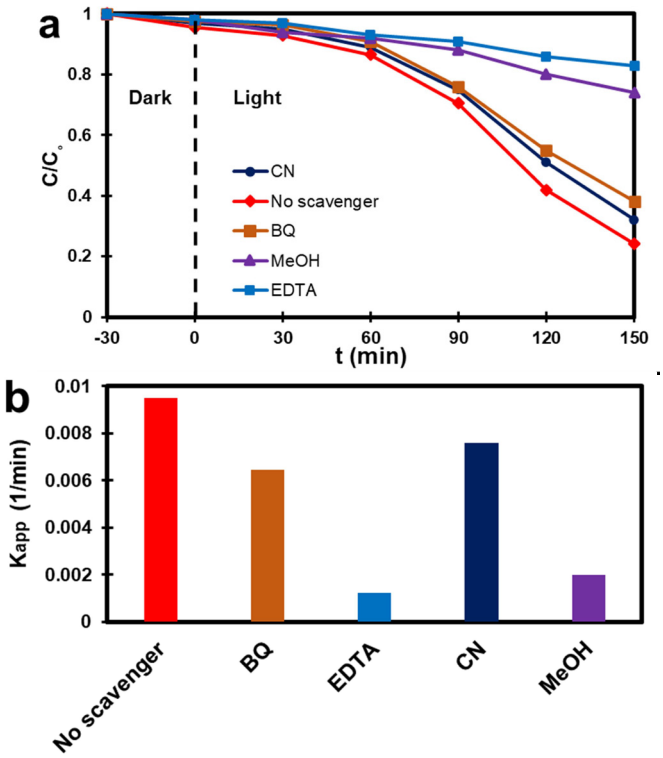

Fig. 8- (a) photocatalytic degradation of MB over the CZ4.5 sample and (b) k_{app} values in the presence of scavengers.

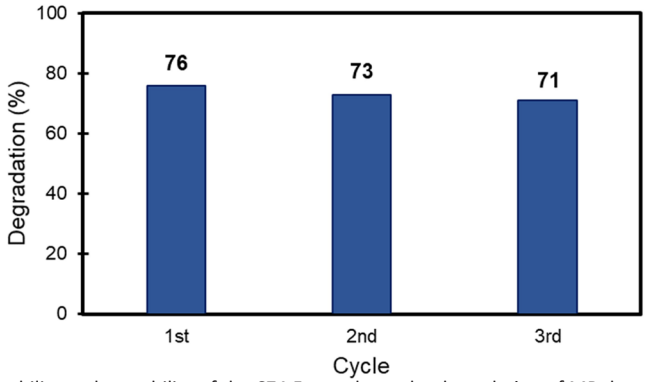

Fig. 9- Stability and reusability of the CZ4.5 sample on the degradation of MB dye over three cycles.

Table1- Comparison of degradation efficiencies of organic dyes using ZnO/CuO nanocomposites as the photocatalyst

No.	Molar ratio of Zn:Cu	Method	Target pollutant	Light source	Performance	Ref.
1	10:1	Chemical bath precipitation	MB	tungsten–halogen lamp (150 W)	76% degradation in 150 min	Present study
2	10:1	Hydrothermal	Triclopyr	Hg lamp (125 W)	79.89% degradation in 100 min	[7]
3	20:1	Solution phase	MB	Xe lamp (500 W)	96.57% degradation in 25 min	[41]
4	49:1	Microwave	Acid Orange 7	Xe lamp (250 W)	80.5% degradation in 120 min	[42]
5	99.5:0.5	Electrospinning	MB	Xe lamp (300 W)	~100% degradation in 120 min	[10]

The photostability and reusability of the CZ4.5 sample have been studied by recycling the sample for three cycles. As shown in Fig. 9, the degradation efficiency of MB decreased from 76% in the first cycle to 71% in the third one. Accordingly, a slight shift was observed in the photocatalytic degradation after three rounds of testing. This, may be due to the loss of the photocatalyst powder during each round of collection and reuse. It is worth mentioning that the catalyst retained its original color after washing and drying during each run.

It is great to notice that the photocatalytic degradation of organic dyes depends on various factors such as light source, synthesis conditions, target pollutant, etc. [37,38]. For instance, different light sources provide different wavelength emission range for degradation of dyes [39]. Also, diverse synthesis conditions such as temperature and pH can influence the solubility of the obtained catalyst and affect the kinetics of the photocatalytic reactions [40]. Table 1 briefly displays a comparison between the degradation efficiencies of ZnO/CuO nanocomposite in recent experimental studies based on the mentioned factors.

4. Conclusion

In summary, ZnO/CuO nanocomposites with different pH values were synthesized through the facile chemical bath precipitation method. To find out the effect of the synthesis pH, different characterization techniques were employed. The structural and morphological properties were investigated by FESEM and XRD. Additionally, the DRS results show that the band gap energy of the CZ4.5 sample is smaller than the sample synthesized at a lower pH value. Further investigation such as PL was considered on the optical properties. The PL spectra indicate the reduction of electron-hole recombination rate in the CZ4.5 sample. Thus, an enhanced visible absorption was observed in the CZ4.5 sample due to the optical investigations. Photo-degradation performance of ZnO/CuO nanocomposites revealed that the degradation efficiency of MB in the CZ4.5 sample after 150 min is ~76% which is higher than the one for the CZ1.5 sample. The photocatalyst dosage was increased from 500 mg/L to 600 and 700 mg/L and the maximum photocatalytic efficiency was first increased to 94% and decreased at the higher dosage. The holes and hydroxyl radicals were found to be important elements for the photocatalytic mechanism over the synthesized sample. The photocatalytic efficiency of the optimized sample (CZ4.5) indicated no notable losses after three cycles. It seems that the CZ4.5 sample can be a good candidate for effective removal of pollutants in wastewater treatment.

References

1. Munawar T, Yasmeen S, Hussain A, Akram M, Iqbal F. Novel direct dual-Z-scheme ZnO-Er2O3-Yb2O3 heterostructured nanocomposite with superior photocatalytic and antibacterial activity. Materials Letters. 2020;264:127357.
2. Saad AM, Abukhadra MR, Abdel-Kader Ahmed S, Elzanaty AM, Mady AH, Betiha MA, et al. Photocatalytic degradation of malachite green dye using chitosan supported ZnO and Ce–ZnO nano-flowers under visible light. Journal of Environmental Management. 2020;258:110043.
3. Das D, Karmakar L. Optimization of Si doping in ZnO thin films and fabrication of n-ZnO:Si/p-Si heterojunction solar cells. Journal of Alloys and Compounds. 2020;824:153902.
4. Rahman F. Zinc oxide light-emitting diodes: a review. Optical Engineering. 2019;58(01):1.
5. Li H, Zhao L, Meng J, Pan C, Zhang Y, Zhang Y, et al. Triboelectric-polarization-enhanced high sensitive ZnO UV sensor. Nano Today. 2020;33:100873.
6. Mahajan P, Singh A, Arya S. Improved performance of solution processed organic solar cells with an additive layer of sol-gel synthesized ZnO/CuO core/shell nanoparticles. Journal of Alloys and Compounds. 2020;814:152292.
7. Kumari V, Sharma S, Sharma A, Kumari K, Kumar N. Hydrothermal synthesis conditions effect on hierarchical ZnO/CuO hybrid materials and their photocatalytic activity. Journal of Materials Science: Materials in Electronics. 2021;32(7):9596-610.
8. Rakhsha AH, Abdizadeh H, Pourshaban E, Golobostanfard MR, Mastelaro VR, Montazerian M. Ag and Cu doped ZnO nanowires: A pH-Controlled synthesis via chemical bath deposition. Materialia. 2019;5:100212.
9. Xu L, Zhou Y, Wu Z, Zheng G, He J, Zhou Y. Improved photocatalytic activity of nanocrystalline ZnO by coupling with CuO. Journal of Physics and Chemistry of Solids. 2017;106:29-36.
10. Naseri A, Samadi M, Mahmoodi NM, Pourjavadi A, Mehdipour H, Moshfegh AZ. Tuning Composition of Electrospun ZnO/CuO Nanofibers: Toward Controllable and Efficient Solar Photocatalytic Degradation of Organic Pollutants. The Journal of Physical Chemistry C. 2017;121(6):3327-38.
11. Nami M, Rakhsha A, Sheibani S, Abdizadeh H. The enhanced photocatalytic activity of ZnO nanorods/CuO nanourchins composite prepared by chemical bath precipitation. Materials Science and Engineering: B. 2021;271:115262.
12. Mwankemwa BS, Nambala FJ, Kyeyune F, Hlatshwayo TT, Nel JM, Diale M. Influence of ammonia concentration on the microstructure, electrical and raman properties of low temperature chemical bath deposited ZnO nanorods. Materials Science in Semiconductor Processing. 2017;71:209-16.
13. Verrier C, Appert E, Chaix-Pluchery O, Rapenne L, Rafhay Q, Kaminski-Cachopo A, et al. Effects of the pH on the Formation and Doping Mechanisms of ZnO Nanowires Using Aluminum Nitrate and Ammonia. Inorganic Chemistry. 2017;56(21):13111-22.
14. Gerbreders V, Krasovska M, Sledevskis E, Gerbreders A, Mihailova I, Tamanis E, et al. Hydrothermal synthesis of ZnO nanostructures with controllable morphology change. CrystEngComm. 2020;22(8):1346-58.
15. Hezam A, Namratha K, Drmosh QA, Chandrashekar BN, Sadasivuni KK, Yamani ZH, et al. Heterogeneous growth mechanism of ZnO nanostructures and the effects of their morphology on optical and photocatalytic properties. CrystEngComm. 2017;19(24):3299-312.
16. Lee M-K, Shih T-H, Chen P-C. Zinc Oxide and Zinc Hydroxide Growth Controlled by Nitric Acid in Zinc Nitrate and Hexamethylenetetramine. Journal of The Electrochemical Society. 2009;156(4):H268.
17. Deng X, Wang C, Shao M, Xu X, Huang J. Low-temperature solution synthesis of CuO/Cu2O nanostructures for enhanced photocatalytic activity with added H2O2: synergistic effect and mechanism insight. RSC Advances. 2017;7(8):4329-38.
18. Azad S, Sadeghi E, Parvizi R, Mazaheri A. Fast response relative humidity clad-modified multimode optical fiber sensor with hydrothermally dimension controlled ZnO nanorods. Materials Science in Semiconductor Processing. 2017;66:200-6.
19. Strano V, Urso RG, Scuderi M, Iwu KO, Simone F, Ciliberto E, et al. Double Role of HMTA in ZnO Nanorods Grown by Chemical Bath Deposition. The Journal of Physical Chemistry C. 2014;118(48):28189-95.
20. Liao A-Z, Zhu W-D, Chen J-B, Zhang X-Q, Wang C-W. Vertically aligned single-crystalline ultra-thin CuO nanosheets: Low-temperature fabrication, growth mechanism, and excellent field emission. Journal of Alloys and Compounds. 2014;609:253-61.
21. Zhang Z, Yi JB, Ding J, Wong LM, Seng HL, Wang SJ, et al. Cu-Doped ZnO Nanoneedles and Nanonails: Morphological Evolution and Physical Properties. The Journal of Physical Chemistry C. 2008;112(26):9579-85.
22. Muhambihai P, Rama V, Subramaniam P. Photocatalytic degradation of aniline blue, brilliant green and direct red 80 using NiO/CuO, CuO/ZnO and ZnO/NiO nanocomposites. Environmental Nanotechnology, Monitoring & Management. 2020;14:100360.
23. Tauc J, Grigorovici R, Vancu A. Optical Properties and Electronic Structure of Amorphous Germanium. physica status solidi (b). 1966;15(2):627-37.
24. Jiang J, Mu Z, Xing H, Wu Q, Yue X, Lin Y. Insights into the synergetic effect for enhanced UV/visible-light activated photodegradation activity via Cu-ZnO photocatalyst. Applied Surface Science. 2019;478:1037-45.
25. Al-Gaashani R, Radiman S, Daud AR, Tabet N, Al-Douri Y. XPS and optical studies of different morphologies of ZnO nanostructures prepared by microwave methods. Ceramics International. 2013;39(3):2283-92.
26. Zhao J-H, Liu C-J, Lv Z-H. Photoluminescence of ZnO nanoparticles and nanorods. Optik. 2016;127(3):1421-3.
27. Zeng H, Duan G, Li Y, Yang S, Xu X, Cai W. Blue Luminescence of ZnO Nanoparticles Based on Non-Equilibrium Processes: Defect Origins and Emission Controls. Advanced Functional Materials. 2010;20(4):561-72.
28. Siddiqui H, Parra MR, Haque FZ. Optimization of process parameters and its effect on structure and morphology of CuO nanoparticle synthesized via the sol–gel technique. Journal of Sol-Gel Science and Technology. 2018;87(1):125-35.
29. Yoon J, Oh S-G. Synthesis of amine modified ZnO nanoparticles and their photocatalytic activities in micellar solutions under UV irradiation. Journal of Industrial and Engineering Chemistry. 2021;96:390-6.
30. Momina, Mohammad S, Suzylawati I. Study of the adsorption/desorption of MB dye solution using bentonite adsorbent coating. Journal of Water Process Engineering. 2020;34:101155.
31. Nami M, Sheibani S, Rashchi F. Photocatalytic performance of coupled semiconductor ZnO–CuO nanocomposite coating prepared by a facile brass anodization process. Materials Science in Semiconductor Processing. 2021;135:106083.
32. Liu B, Yin D, Zhao F, Khaing KK, Chen T, Wu C, et al. Construction of a Novel Z-Scheme Heterojunction with Molecular Grafted Carbon Nitride Nanosheets and V2O5 for Highly Efficient Photocatalysis. The Journal of Physical

Chemistry C. 2019;123(7):4193-203.
33. Ahmed Y, Yaakob Z, Akhtar P. Degradation and mineralization of methylene blue using a heterogeneous photo-Fenton catalyst under visible and solar light irradiation. Catalysis Science & Technology. 2016;6(4):1222-32.
34. Jourshabani M, Lee B-K, Shariatinia Z. From Traditional Strategies to Z-scheme Configuration in Graphitic Carbon Nitride Photocatalysts: Recent Progress and Future Challenges. Applied Catalysis B: Environmental. 2020;276:119157.
35. El-Salamony RA, Hassan SA. Reforming of Rice Ash Waste by Incorporated Nanotitania in Silica Framework for Photo-catalytic Treatment of Wastewater. Applied Organometallic Chemistry. 2020;34(10).
36. Yu W, Liu J, Yi M, Yang J, Dong W, Wang C, et al. Active faceted Cu2O hollow nanospheres for unprecedented adsorption and visible-light degradation of pollutants. Journal of Colloid and Interface Science. 2020;565:207-17.
37. Chen D, Cheng Y, Zhou N, Chen P, Wang Y, Li K, et al. Photocatalytic degradation of organic pollutants using TiO2-based photocatalysts: A review. Journal of Cleaner Production. 2020;268:121725.
38. Viswanathan B. Photocatalytic Degradation of Dyes: An Overview. Current Catalysis. 2018;7(2):99-121.
39. Vaiano V, Sacco O, Stoller M, Chianese A, Ciambelli P, Sannino D. Influence of the Photoreactor Configuration and of Different Light Sources in the Photocatalytic Treatment of Highly Polluted Wastewater. International Journal of Chemical Reactor Engineering. 2014;12(1):63-75.
40. Variar AG, M.S R, Ail VU, S SP, K S, Tahir M. Influence of various operational parameters in enhancing photocatalytic reduction efficiency of carbon dioxide in a photoreactor: A review. Journal of Industrial and Engineering Chemistry. 2021;99:19-47.
41. Bharathi P, Harish S, Archana J, Navaneethan M, Ponnusamy S, Muthamizhchelvan C, et al. Enhanced charge transfer and separation of hierarchical CuO/ZnO composites: The synergistic effect of photocatalysis for the mineralization of organic pollutant in water. Applied Surface Science. 2019;484:884-91.
42. Ruan S, Huang W, Zhao M, Song H, Gao Z. A Z-scheme mechanism of the novel ZnO/CuO n-n heterojunction for photocatalytic degradation of Acid Orange 7. Materials Science in Semiconductor Processing. 2020;107:104835.